Journal Name

Dynamic Article Links ►

Cite this: DOI: 10.1039/c0xx00000x

www.rsc.org/xxxxxx

ARTICLE TYPE

Interests in new heterodinuclear transition-metal/main-group-metal complexes: DFT study of electronic structure and mechanism of fluoride sensing function

Wei Guan, Shinichi Yamabe and Shigeyoshi Sakaki*

Received (in XXX, XXX) Xth XXXXXXXXX 20XX, Accepted Xth XXXXXXXXX 20XX
DOI: 10.1039/b000000x

Systematic DFT calculations were carried out on a series of heterodinuclear complexes [(*o*-$(Ph_2P)C_6H_4)_3M^1M^2Cl]^+$ (M^1 = As, Sb, or Bi; M^2 = Pd or Pt) to investigate the mechanism of colorimetric sensing function for fluoride anion. Fluoride anion binds with the M^1 center to afford a hypervalent M^1 species with large stabilization energy. For instance, the stabilization energy by the fluoride adduct formation is −15.5 kcal mol^{-1} for **3** (M^1 = Sb; M^2 = Pd) and −16.2 kcal mol^{-1} for **6** (M^1 = Sb; M^2 = Pt), where a negative value represents stabilization. Interestingly, the allosteric coordination of the third phosphine with the M^2 center is induced by the fluoride adduct formation. For chloride, bromide, and thiocyanide anions, the binding energies are positive (~4.5 kcal mol^{-1}), and the allosteric coordination does not occur. The allosteric coordination plays a crucial role in absorption spectrum change induced by the fluoride adduct formation. For instance, the fluoride adduct formation quenches the absorption band of **3** around 400 nm and newly exhibits two absorption peaks at longer wavelength, 475 and 451 nm. These two peaks are assigned to ligand-field transitions ($d_{xy} \rightarrow d_{z^2}$ and $d_{x^2-y^2} \rightarrow d_{z^2}$) including metal-to-ligand charge transfer character. We discussed the reasons why the allosteric coordination can occur only in the fluoride adduct and induces these two absorptions in the longer wavelength region. In addition, the Bi-Pd combination is also recommended for a fluoride sensing material, while the Sb-Pt combination is recommended for cyanide sensing.

Introduction

Fluoride anion plays a crucial role in biological process and also our daily life.[1] For instance, its excessive intake leads to dental and skeletal fluorosis and even osteosarcoma.[2,3] In this regard, the detection and the sensing of the anion are necessary.[4-8] Among various available recognition and sensing strategies, hydrogen bonding with fluoride anion is utilized for selective sensing function of amide, urea, thiourea, guanidinium and pyrrole derivatives.[9-17] However, the drawback of this strategy is that most of the sensors can detect the anion only in organic media. In contrast to them, the polyfunctional main-group Lewis acids are expected to be an alternative sensing platform, because they are capable of strongly binding various anions. The sensing mechanism of such Lewis acids is different from the common one observed for Brønsted acid-base reactions.[18-20] Among Lewis acids, the sensing for fluoride by organoboranes and related derivatives has been widely investigated.[21-25] They are not only able to present greater binding capacity with fluoride anion but also to provide detectable photophysical change by the binding. This is an important merit of Lewis acid sensing materials. However, such complexes are in general unstable or even easily decomposed in the presence of water due to the large hydration energy of the anion. This disadvantage inevitably limits the scope of their application. In other words, a good fluoride chemosensor must exhibit hydrolytic stability, as well as large ion affinity, high selectivity, and visible photophysical response. One strategy to satisfy these conditions is to utilize transition metals for building up the fluoride sensors. The strategy is guided by the expectation that transition metals assist anion binding interaction without exerting any direct interaction with the guest anion and provide the detectable photophysical signal.[26]

Based on above expectations, Wade et al. recently synthesized a hetero dinuclear stibine-palladium complex [(*o*-$(Ph_2P)C_6H_4)_3SbPdCl]^+$ and found that it is useful for visual detection of fluoride anion with high selectivity.[27] An attractive aspect is the geometry change of the palladium center from a square-planar to a trigonal-bipyramidal structure by the formation of fluoride adduct, as shown in Scheme 1. The authors discussed that the geometry change is responsible to the appearance of intense ligand-field transition by the fluoride adduct formation and the appearance of new absorption band is crucial for colorimetric sensing. The compounds were investigated by X-ray diffraction, NMR spectroscopy, and UV/vis spectra. However, there are several important questions: (1) What is the role of the transition-metal in sensing fluoride anion? (2) What is the sensing mechanism that really controls the observed color change? (3) What is the origin of high selectivity for fluoride anion? (4) Why

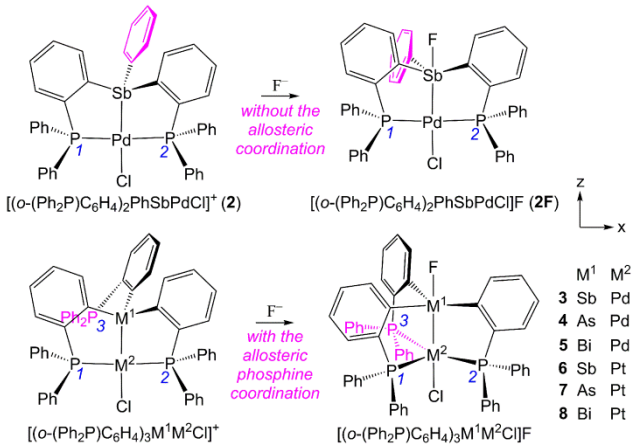

Scheme 1 Heterodinuclear transition-metal (M^2)/main-group-metal (M^1) complexes investigated in this work.

is the allosteric coordination of the third phosphine induced by the fluoride addition but cannot occur in the absence of fluoride anion?

Complexes including the interaction between transition-metal and hypervalent heavy main-group element have been reported a long time ago by Akiba group;[28] for instance, group 6, 8 and 10 transition metal complexes with hypervalent antimony and phosphorus species were synthesized. Besides, group 6, 10 and 12 transition metal complexes with hypervalent silicon and tin species were recently reported.[29-32] Though all these complexes are interesting from the viewpoint of bonding nature and electronic structure, they have not been used as a sensing material. Also, theoretical studies of these transition metal complexes with main group hypervalent species have been limited.[20,33,34] In this regard, it is of considerable importance to elucidate the mechanism of fluoride sensing function of the heterodinuclear Sb/Pd complex based on theoretical knowledge of the bonding nature.

In the present work, we performed systematic density functional theory (DFT) calculations on a series of heterodinuclear main-group/transition-metal complexes $[(o\text{-}(Ph_2P)C_6H_4)_3M^1M^2Cl]^+$ (M^1 = As, Sb, or Bi; M^2 = Pd or Pt). Our purposes here are to provide theoretical answers to the above four questions and to predict theoretically other fluoride sensing complexes. The interaction between transition-metal and hypervalent species is interesting but has not been theoretically investigated well. Hence, it is also our purpose to provide theoretical knowledge of the bonding nature between transition-metal and hypervalent Sb species.

Computational methods

All calculations[35] were performed with the Gaussian09 program package[36] at the DFT level. After careful benchmark test performed in this work, the PBE0[37-39] hybrid exchange correlation functional was used throughout this work. Results of the performance of geometry optimization are shown in Tables S1-S4 of ESI. Each stationary structure was verified by vibrational frequency calculation. Two kinds of basis set system were employed here. In basis set I (BS-I), (541/541/211/1), (541/541/21/1)[40,41] and (21/21/1)[42] basis sets were employed for transition metals (Pd and Pt) and main group heavy atoms (As, Sb and Bi), respectively, with Los Alamos relativistic effective core potentials (ECPs).[43-45] For H, B, C, N, Si, P, S, F, Cl, and Br atoms, 6-31G(d) basis sets were employed, where one diffuse function was added for each of P and halogen atoms. At this level, the experimental structural parameters were well reproduced; see Tables S5-S7. All of the TD-DFT and single point calculations were carried out with a better basis set system (BS-II). In BS-II, (5311/5311/211/1) and (5311/5311/21/1) basis sets were employed for Pd and Pt respectively with the Los Alamos ECPs. Aug-cc-pVTZ-PP[46] basis sets were used for As, Sb, and Bi with relativistic ECPs.[47] cc-pVDZ[48] basis sets were used for H, B, C, N, and S atoms, while aug-cc-pVDZ[48-50] basis sets were employed for P and halogen atoms. Solvent effects of CH_2Cl_2 were evaluated with the polarizable continuum model (PCM),[51] where the so-called non-equilibrium approach was employed because it is designed for the photo-excitation process. The absorption spectra were simulated by using GaussSum program Rev. 2.2[52] with the full width at half maximum (FWHM) of 3000 cm^{-1} based on the present TD-DFT computational results.

Results and discussion

1. Structures of 2, 3 and their fluoride adducts. First, two of stibine complexes and their fluoride adducts, $[(o\text{-}(Ph_2P)C_6H_4)_2PhSbPdCl]^+$ (**2**), $[(o\text{-}(Ph_2P)C_6H_4)_2PhSbPdCl]F$ (**2F**), $[(o\text{-}(Ph_2P)C_6H_4)_3SbPdCl]^+$ (**3**), and $[(o\text{-}(Ph_2P)C_6H_4)_3SbPdCl]F$ (**3F**), were investigated, as shown in Fig. 1; note that **2** and **2F** include two phosphine groups in the Sb moiety and **3** and **3F** include three phosphines (Scheme 1). For the comparisons, a non-transition-metal compound Ph_4Sb^+ (**1**) and its fluoride adduct Ph_4SbF (**1F**) were investigated. In **2** and **3**, the Pd center takes a pseudo-square-planar four-coordinate structure, as reported experimentally.[27] The Sb-C bonds of **2** and **3** are longer than in **1** (2.105 Å) by 0.013~0.046 Å, probably due to the presence of the Pd-Sb coordination bond. In **3**, the presence of the third bulky PPh_2 moiety (P3 moiety, *i.e.*, PPh_2-3) induces moderate expansion of the framework; for instance, see the Sb-C4 distance of 2.151 Å in **3** and 2.132 Å in **2**. Also, the Pd-Sb-C5 angle (136.6°) is larger in **3** than in **2** (125.9°). In the fluoride adducts, the Sb-F bond length is 2.052 Å and 2.047 Å in **2F** and **3F**, respectively. They are little different from that of **1F**, indicating that the Sb-F distance depends on the substituent at the *trans* position little. The formation of the Sb-F bond changes the tetrahedral coordination geometry of the Sb center (**1**, **2**, and **3**) to a trigonal-bipyramidal one (**1F**, **2F**, and **3F**). The Wiberg Sb-C bond index decreases by the fluoride addition; see Table S8. Consistent with this change, the average Sb-C bond is moderately elongated by 0.02~0.04 Å in **1F**, **2F** and **3F**. The Pd-Cl and Pd-Sb bonds of **2F** and **3F** are longer than in **2** and **3**. The Pd-P1 and Pd-P2 distances become smaller in **2F** than in **2**, while they become larger in **3F** than in **3**. All these geometrical changes may not be easily explained by a single factor but by the combination of the electronic effects, the structural effects and the allosteric coordination of the third phosphine, as will be discussed below.

2. Electronic process in the formation of fluoride adduct. When going from **1** to **1F**, the Sb atomic population decreases by 0.174*e* and electron populations of all phenyl groups increase, as shown in Table 1; in particular, the electron population of the Ph4 group increases by 0.179*e* more than those of other phenyl

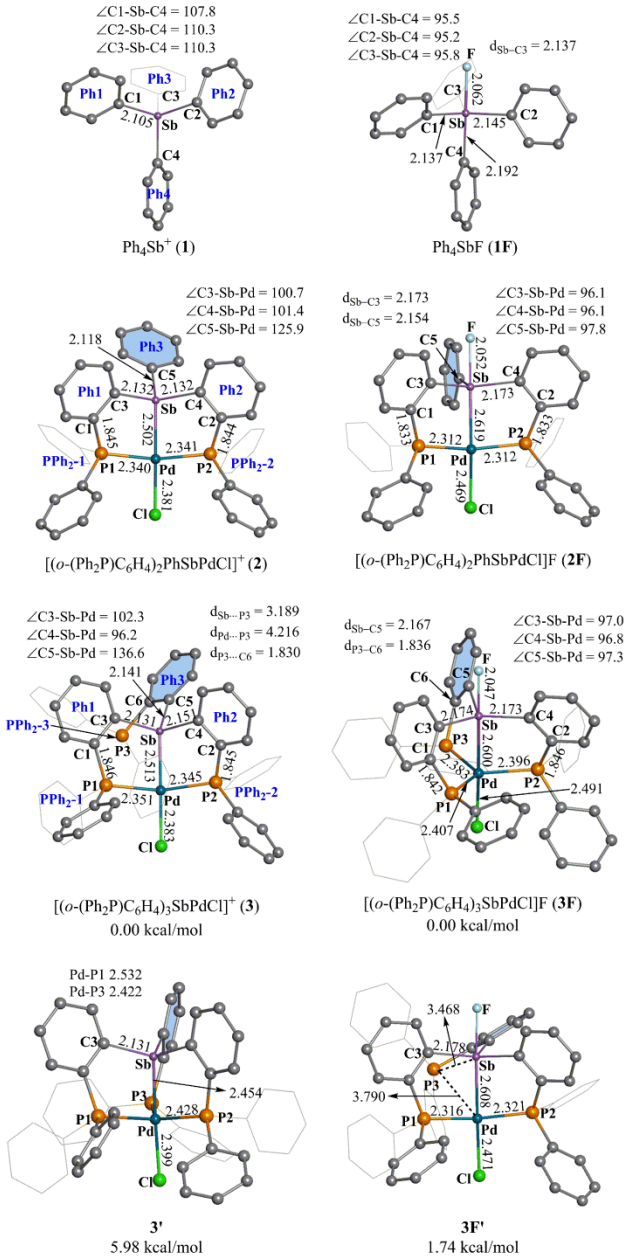

Fig. 1 Optimized structures and selected geometrical parameters (bond length in Angstrom unit and bond angle in degree) of **1**, **1F**, **2**, **2F**, **3**, **3F**, **3'**, and **3F'** calculated at the PCM(CH_2Cl_2)/PBE0/BS-I level. Relative energies (in kcal mol^{-1}) were calculated at the PCM(CH_2Cl_2)/PBE0/BS-II//PCM/PBE0/BS-I level. Hydrogen atoms of benzene rings are omitted for clarity. Phenyl groups located at the back side are shown by faint black colors. In **3'** and **3F'**, the allosteric coordination is present and absent, respectively.

groups. These results clearly indicate that the adduct formation of fluoride enhances the donating ability of the Sb atom and the substituent at the position *trans* to the fluoride is influenced much more by the adduct formation than others. When going from **2** to **2F**, the Sb atomic population similarly decreases, indicating that the Sb atom becomes more electron-donating in **2F**. The electron population of the Pd-Cl moiety somewhat increases by 0.138*e* like the Ph4 electron population in **1F**. This indicates that because the Sb moiety becomes more electron-donating the σ-donation of the Cl ligand is suppressed in **2F**, which is the origin of the Pd-Cl elongation in **2F**. The electron populations of the PPh_2-1 and PPh_2-2 moieties also increase by 0.109*e* in **2F**, respectively, suggesting that the σ-donation of phosphine becomes weaker in **2F**. This is against the Pd-P1 and Pd-P2 bond shortening by about 0.03 Å. It is likely that this unexpected result arises from the chelating structure of (*o*-(Ph_2P)C_6H_4)$_2$PhSb ligand, as follows: In the fluoride adduct, the Sb center takes a trigonal-bipyramidal structure, in which the Ph group on the Sb moves downward, as shown by the decrease in the Pd-Sb-C5 angle to 97.8° in **2F** from 125.9° in **2** (Fig. 1). Hence, the Ph moiety must approach the Pd center.

To ascertain the above explanation, we investigated a model complex $\mathbf{2_m}$ and its fluoride adduct $\mathbf{2_mF}$, in which the phosphine moiety is not bound with the Sb moiety and the simplest PH_3 was employed to avoid steric effect, as shown in Fig. S1. Though the Pd-Cl and Pd-Sb distances change similar to those in the **2** → **2F** conversion, the Pd-P distance becomes shorter in the $\mathbf{2_m}$ → $\mathbf{2_mF}$ conversion to a much lesser extent than in the **2** → **2F** conversion. These results indicate that the chelating structure of (*o*-(Ph_2P)C_6H_4)$_2$PhSb is one of the important factors for the Pd-P bond shortening induced by the **2** → **2F** conversion.[53]

In **3F**, the similar population changes are observed in the Sb, P1, P2 and Cl atoms, while the p electron population of the Pd center considerably increases by 0.559*e* in Table 1. This increase in the Pd p orbital population arises from the allosteric coordination of the third phosphine, as follows: In **3F**, the P1, P2, and P3 phosphines coordinate with the Pd center in the *xy* plane; see Scheme 1 for *x*, *y*, and *z*-axes. Because the d_{z^2} orbital is unoccupied in a formal sense in the trigonal-bipyramidal d^8 complex, three phosphines must interact with $4d_{z^2}$, and outer 5*s*, $5p_x$ and $5p_y$ orbitals. However, the $4d_{z^2}$ orbital has larger lobes along the *z*-axis and smaller one on the *xy* plane. Hence, it mainly interacts with the Sb and Cl and moderately with three phosphines. As a result, the three phosphines mainly interact with the Pd 5*s*, $5p_x$ and $5p_y$ orbitals. This leads to considerable increase in the p orbital population. Also, the Pd-P coordinate bonds become considerably weaker in the trigonal-bipyramidal d^8 structure than those of **3**. The similar changes in electron population and Pd-P distance are observed in model complexes; see the geometrical changes (Fig. S1) and the natural population changes (Table S9).

In addition, the interaction between transition-metal and hypervalent species is of considerable interest but it has not been investigated well. Hence, we investigated the donating ability and the *trans*-influence of the hypervalent Sb species, because these are important in the coordination chemistry. The model complex $\mathbf{2_m}$ is compared with its Si analogue, [PdCl($SiPh_3$)(PH_3)$_2$] ($\mathbf{2_mSi}$), because the $SiPh_3$ ligand is strongly-donating and its *trans*-influence is strong, as is well known. The Pd-Cl distance (2.376 Å) of $\mathbf{2_m}$ is considerably shorter than that of $\mathbf{2_mSi}$ (2.489 Å), indicating that the *trans*-influence of $SbPh_3$ is weaker than those of $SiPh_3$; see Fig. S1. Consistent with the results of *trans*-influence, the donation from $SiPh_3$ is stronger than that from $SbPh_3$; see the electron population of the PdCl(PH_3)$_2$ moiety in Table S9. However, in $\mathbf{2_mF}$, the Pd-Cl distance is moderately longer than that of $\mathbf{2_mSi}$, and the electron population of the PdCl(PH_3)$_2$ moiety is larger in $\mathbf{2_mF}$ than in $\mathbf{2_mSi}$. These results clearly indicate that the hypervalent Sb moiety exhibits stronger

Table 1 Natural Population of **1**-**3** and their fluoride adducts[a]

		1 + F^-	**1F** [Δ(**1F**-**1**)][b]	**2** + F^-	**2F** [Δ(**2F**-**2**)][b]	**3** + F^-	**3F** [Δ(**3F**-**3**)][b]	**3'**
Pd	s			8.501	8.519 [0.018]	8.480	8.444 [–0.036]	8.448
	p			18.581	18.505 [–0.076]	18.501	19.060 [0.559]	19.070
	d			19.366	19.429 [0.063]	19.361	19.399 [0.038]	19.347
	total			46.448	46.453 [0.005]	46.342	46.903 [0.561]	46.865
Sb		48.791	48.617 [–0.174]	49.190	48.915 [–0.275]	49.272	48.795 [–0.477]	49.049
Ph[c]		41.302	41.382 [0.080]	40.840	40.893 [0.053]	40.629	40.661 [0.032]	40.617
Ph4		41.302	41.481 [0.179]					
P[d]				13.817	13.855 [0.038]	13.837	13.861 [0.024]	13.857
P3						14.091	13.837 [–0.254]	13.820
PPh_2[e]				96.204	96.313 [0.109]	96.235	96.369 [0.134]	96.298
PPh_2-3						96.575	96.327 [–0.248]	96.238
Cl				17.435	17.568 [0.133]	17.453	17.498 [0.045]	17.400
F		10.000	9.756	10.000	9.760	10.000	9.757	

a The PCM(CH_2Cl_2)/PBE0/BS-I geometries. *b* The difference in population between **nF** and **n** (**n** = **1**, **2**, or **3**). A negative value means decrease in population when going from **n** to **nF**. *c* Average value of Ph1, Ph2 and Ph3. *d* Average value of P1 and P2. *e* Average value of PPh_2-1 and PPh_2-2.

donation ability and stronger *trans*-influence than the $SiPh_3$ ligand.

3. The reasons for the allosteric coordination of the third phosphine with the Pd center in the fluoride adduct. One of the interesting features in the **3** → **3F** conversion is that the allosteric coordination of the third phosphine P3 with the Pd center is induced by the fluoride addition. Because this is crucial for colorimetric detection of fluoride anion, as will be discussed below, it is of considerable importance to elucidate the reason why the third phosphine coordinates with the Pd center not in **3** but in **3F**. As the first step, we investigated whether the phosphine coordinates with the Pd center in **3** (*i.e.*, without F^-) or not. As shown in Fig. 1, we constructed a model complex **3'** and optimized its geometry in which the Pd-P3 distance is in the range of the usual Pd-P coordinate bond one. The optimized Pd-P3 distance of 2.422 Å is somewhat shorter than the Pd-P1 and similar to the Pd-P2 distance, indicating that the Pd-P3 bonding interaction is formed in **3'**. The electron populations of **3'** are considerably different from those of **3**, as shown in Table 1. In particular, the large p orbital population (19.070*e*) of the Pd is found. This is consistent with the trigonal-bipyramidal d^8 complex; see above. Despite of the presence of the additional Pd-P3 coordinate bond, **3'** is more unstable than **3** by 5.98 kcal mol^{-1}. It clearly indicates that the third phosphine does not coordinate with the Pd center when fluoride is absent. Two model systems $[PdCl(SbPh_3)(PH_3)_3]^+$ (**3m**) and **3mF** were calculated here to investigate the effect of the bridging structure of (*o*-$(Ph_2P)C_6H_4)_3Sb$, as shown in Fig. S1. In **3m**, the Pd-P3 distance is much longer than the other Pd-P distances. The model **3m** is moderately more stable than **2m** + PH_3 by 1.57 kcal mol^{-1}, indicating that the P3 coordination in **3m** is a thermodynamically favourable process. These differences between **3m** and **3'** suggest that the chelating structure of the (*o*-$(Ph_2P)C_6H_4)_3Sb$ moiety gives rise to a considerably large destabilization energy of **3'** when the allosteric coordination of the P3 phosphine occurs. Certainly, the (*o*-$(Ph_2P)C_6H_4)_3Sb$ moiety in **3'** is much more unstable than in **3** by 18.31 kcal mol^{-1}. This strain energy is larger than the stabilization by the coordination of the third phosphine, which is about 12.33 kcal mol^{-1}.[54] Hence, it should be concluded that the P3 phosphine does not coordinate with the Pd center in the absence of fluoride anion. We investigated the fluoride adduct **3F'** without the allosteric coordination, in which the Pd-P3 distance (3.790 Å) is considerably larger than the usual coordinate bond. Interestingly, **3F** is moderately more stable than **3F'** by 1.74 kcal mol^{-1}. The (*o*-$(Ph_2P)C_6H_4)_3SbF$ moiety in **3F** is a little bit more unstable than in **3F'** by 3.44 kcal mol^{-1}, indicating that the strain energy becomes very small in **3F**. Because this moderate strain energy is overcome by the Pd-P3 coordinate bond, the allosteric coordination of the third phosphine occurs in **3F**. In a model system, on the contrary, **3mF** is moderately less stable than **2mF** + PH_3. This indicates that the coordination of the third phosphine does not occur in a model system even in the fluoride adduct. In the model system, the phosphine moiety is not connected with the Sb moiety. These results suggest that the chelating structure of the (*o*-$(Ph_2P)C_6H_4)_3Sb$ ligand is responsible for the allosteric coordination of the third phosphine in **3F**.

The next issue to be elucidated is the reason why the chelating structure of the (*o*-$(Ph_2P)C_6H_4)_3SbF$ moiety is necessary for the allosteric coordination. When the fluoride adduct is formed, the C5-Sb-Pd angle decreases to 97.3° from 136.6° in **3**. In such geometry, the P3 atom can take a position on the equatorial plane of the trigonal-bipyramidal structure. Because this geometry is close to that in **3F**, the coordination of the P3 phosphine can occur with a smaller energy loss in the fluoride adduct **3F** than in **3**. It should be concluded that the chelating structure of (*o*-$(Ph_2P)C_6H_4)_3Sb$ is the origin of the absence of the P3 allosteric coordination in **3** but the presence of the P3 coordination in **3F**; in other words, the chelating structure of the Sb moiety plays a crucial role in the allosteric coordination.

Table 2 The reaction energy for anion-capturing (ΔE, in kcal mol^{-1}) calculated at the PCM(CH_2Cl_2)/PBE0/BS-II//PCM/PBE0/BS-I level

entry	M^1	M^2	model reaction	(ΔE)
1	Sb		[**1**]BMe_4 + [NMe_4]F → **1F** + [NMe_4]BMe_4	–20.8
2	Sb	Pd	[**2**]BMe_4 + [NMe_4]F → **2F** + [NMe_4]BMe_4	–18.5
3	Sb	Pd	[**3**]BMe_4 + [NMe_4]F → **3F** + [NMe_4]BMe_4	–15.5
4	As	Pd	[**4**]BMe_4 + [NMe_4]F → **4F** + [NMe_4]BMe_4	4.2
5	Bi	Pd	[**5**]BMe_4 + [NMe_4]F → **5F** + [NMe_4]BMe_4	–10.5
6	Sb	Pt	[**6**]BMe_4 + [NMe_4]F → **6F** + [NMe_4]BMe_4	–16.2
7	As	Pt	[**7**]BMe_4 + [NMe_4]F → **7F** + [NMe_4]BMe_4	4.2
8	Bi	Pt	[**8**]BMe_4 + [NMe_4]F → **8F** + [NMe_4]BMe_4	–10.9
9	Sb	Pd	[**3**]BMe_4 + [NMe_4]Cl → **3Cl'**[a] + [NMe_4]BMe_4	6.0
10	Sb	Pd	[**3**]BMe_4 + [NMe_4]Br → **3Br'**[a] + [NMe_4]BMe_4	4.3
11	Sb	Pd	[**3**]BMe_4 + [NMe_4]CN → **3CN'**[a] + [NMe_4]BMe_4	–9.9
12	Sb	Pd	[**3**]BMe_4 + [NMe_4]SCN → **3SCN'**[a] + [NMe_4]BMe_4	3.1
13	Bi	Pd	[**5**]BMe_4 + [NMe_4]CN → **5CN'**[a] + [NMe_4]BMe_4	–8.3
14	Sb	Pt	[**6**]BMe_4 + [NMe_4]CN → **6CN** + [NMe_4]BMe_4	–10.3

a Four-coordinate Pd structure without the allosteric phosphine coordination.

4. Other combination of Lewis acids and transition-metal centers. It is of great interest to investigate if the fluoride sensing can be achieved by other combinations of main-group Lewis acids and transition-metal elements. Such knowledge is indispensable to design a new system for fluoride sensing. We investigated **4**-**8** and their fluoride adducts shown in Scheme 1. The fluoride adduct formations of **4**-**8** show similar structural changes to those of the **3** → **3F** conversion; see Fig. S2 and S3 in ESI for these complexes. In order to confirm if the above-mentioned allosteric coordination of phosphine also occurs in these complexes, geometries of two isomers with and without the allosteric coordination were optimized. In all these complexes, the structure with the allosteric phosphine coordination is moderately more stable than that without the allosteric coordination; see **4F'**-**8F'** and **4F**-**8F** in Fig. S4. These results suggest that these analogues are considered to be a candidate of a fluoride sensing material. The next issue to be investigated is the binding energy provided by the formation of the fluoride adduct.

5. Energy stabilization by the formation of fluoride adduct. The binding energy of fluoride anion with those complexes **1**-**8** was evaluated in the presence of counter ions, as shown in Table 2. In the experimental conditions, the tetra-phenylborate (TPB) anion is involved as a counter ion of cationic complexes (**2** and **3**) and the tetra-n-butylammonium (TBA) cation is involved as a counter ion of fluoride anion.[27] The neglect of those counter cation and anion would lead to the overestimation of binding energy. Here, $[BMe_4]^-$ and $[NMe_4]^+$ were employed as models of the counter anion and cation, respectively, to reduce the computational cost. For these computational details, see ESI.

As seen in Table 2, the entries 1-3 are exothermic; the exothermicity decreases in the order **1** (–20.8) > **2** (–18.5) > **3** (–15.5 kcal mol^{-1}), where a negative value indicates stabilization in energy. This is consistent with the Lewis acidity of the Sb center; the Sb positive charge decreases in the order **1** > **2** > **3** (Table 3).

Table 3 Natural charges of **1**-**8**[a]

M^2	none	Pd				Pt		
M^1	Sb	Sb	Sb	As	Bi	Sb	As	Bi
	1	**2**	**3**	**4**	**5**	**6**	**7**	**8**
M^1	2.21	1.81	1.73	1.41	1.62	1.87	1.53	1.76
M^2		–0.45	–0.34	–0.29	–0.31	–0.67	–0.57	–0.64
P1		1.18	1.16	1.16	1.15	1.23	1.24	1.22
P2		1.18	1.17	1.19	1.16	1.24	1.25	1.23
P3			0.91	0.90	0.90	0.90	0.88	0.89
Cl		–0.44	–0.45	–0.45	–0.44	–0.36	–0.36	–0.35

a The PCM(CH_2Cl_2)/PBE0/BS-I geometries

In the As analogue, the binding energy is positive (repulsive); see entry 4 of Table 2. In the Bi analogue, the binding energy is somewhat smaller than that of the Sb-Pd combination; see entry 5 in Table 2. As shown in entries 6-8, the Sb-Pt and Bi-Pt combinations provide moderately larger binding energies than the Pd analogues, while the As-Pt combination presents the similar positive binding energy to that of the As-Pd pair. The very small affinity of the As analogue is consistent with the smaller positive charge on the As center (in **4** or **7**, Table 3). Based on these results, it is concluded that the Sb-Pd/Pt combination is the best as M^1-M^2, the Bi-Pd/Pt is the next, and the As-Pd/Pt cannot be applied to fluoride sensing.

6. Important electronic factor for binding energy of fluoride adduct. The NBO analysis clearly shows that the positive charge of Sb decreases monotonously from **1** (2.21*e*) to **3** (1.73*e*); see Table 3. Though the positive charge of the Sb center is smaller in **2** and **3** than in **1** (see the detailed discussion in ESI), the coordinate bond plays a crucial role in capturing a fluoride anion. Actually, neutral $SbPh_3$ cannot form a fluoride adduct at all; see Fig. S5.

The smaller Lewis acidity in **3** than in **2** is attributed to the presence of the PPh_2 group at the *ortho* position of the Ph group bound with the Sb center. This PPh_2 group is positively charged (0.43*e*), indicating that it is electron-donating. As a result, the Lewis acidity of the Sb center is weaker in **3** than in **2**.

The As and Bi centers of **4** and **5** are less positively charged than the Sb of **3**. The Pauling electronegativity increases in the order Bi (2.02) < Sb (2.05) < As (2.18). The smaller positive charge of the As center arises from its larger electronegativity. However, the smaller positive charge of the Bi than that of the Sb cannot be explained in terms of its smaller electronegativity. In M^1Ph_3 (M^1 = As, Sb, or Bi), the M^1 atomic charge decreases in the order Sb (1.26) > Bi (1.24) > As (1.05), where in parenthesis is the NBO atomic charge. In both of M^1Ph_3 and $[(o\text{-}(Ph_2P)C_6H_4)_3M^1PdCl]^+$, the Bi atomic charge is smaller than the Sb despite of the moderately smaller electronegativity of Bi than that of Sb. One reason is the longer Bi-Ph and Bi-Pd distances than the Sb-Ph and Sb-Pd distances, which induces smaller overlaps between Bi and Ph and between Bi and Pd. Accordingly, the CTs from the Bi to Ph and Pd become smaller than those from the Sb to Ph and Pd. As a result, the Sb atomic charge is moderately more positive than the Bi charge in the Pd complexes, while it is not different very much in M^1Ph_3. It is likely that not only the Pauling electronegativity but also covalent radius is an

important factor for the electron distribution.

The replacement of Pd (2.20) by Pt with higher electronegativity (2.28) in **3**-**5** increases M^1-Pt bond polarity and accordingly increases the positive charge of the M^1 center in **6**-**8**. Especially, the Sb center in **6** has much larger positive charge of 1.87*e* than 1.73*e* in **3** (Table 3). This means that the introduction of Pt enhances the Lewis acidity of the M^1 center and facilitates the capturing fluoride anion, as clearly shown by the larger binding energy of –16.2 kcal mol^{-1} in entry 6 of Table 2.

7. Selectivity for other anions such as chloride, bromide, cyanide, and thiocyanide. The selectivity of **3** for fluoride anion is an important factor to a good sensor for fluoride anion. The binding energy was calculated with chloride, bromide, cyanide, and thiocyanide anions, as listed in Table 2. The formation of chloride, bromide, and thiocyanide adducts are endothermic; see entries 9, 10, and 12 in Table 2. Though the formation of cyanide adduct (entry 11) is exothermic, the exothermicity is much less than the formation of fluoride adduct (entry 3). Thus, it is concluded that **3** is highly selective for a fluoride anion, which is in agreement with the experimental report.[27]

It should be noted here that the allosteric coordination of the third phosphine with the Pd center does not occur in these anion adducts and the Pd center persists in taking a four-coordinate

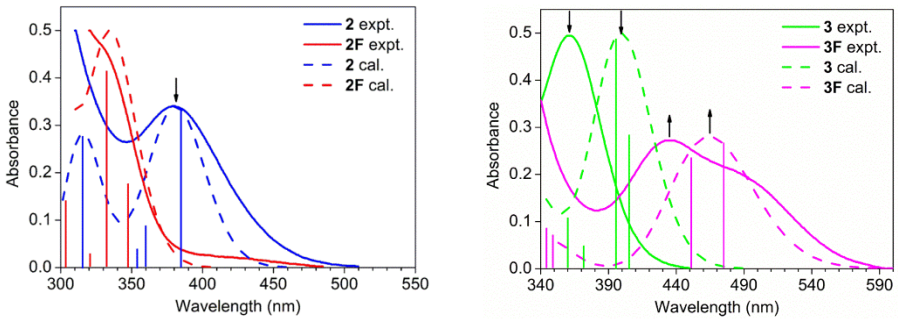

(A) (B)

Fig. 2 Comparisons of experimental[a] and calculated absorption spectra[b] of **2**, **2F**, **3**, and **3F**. *a* Ref. 27. *b* PCM(CH_2Cl_2)/TD-PBE0/BS-II level.

Table 4 Absorption peaks (λ_{abs}) [in eV (nm)], the oscillator strength (*f*), and assignments at the PCM(CH_2Cl_2)/TD-PBE0/BS-II level

complexes	λ_{abs}	major contributions	*f*	assignments	expt.[b]
2	3.24 (383)	H → L[a] (84%)	0.1231	LFT/LMCT	3.25 (381)
	3.45 (360)	H-1 → L (53%) H-12 → L (20%) H-3 → L (16%)	0.0227	LFT/LMCT	
	3.52 (353)	H-3 → L (56%) H-1 → L (20%)	0.0033	LFT/LMCT	
	3.94 (315)	H-2→ L (74%)	0.1108	LFT/LMCT	
2F	3.57 (348)	H → L (71%)	0.0565	LFT	
	3.74 (332)	H-1 → L (86%)	0.1356	LFT/LMCT	
	3.87 (321)	H-3 → L (68%) H-2 → L (14%)	0.0010	LFT/LMCT	
	4.11 (302)	H-2 → L (46%) H → L+2 (17%) H → L (16%)	0.0389	LFT/LMCT	
3	3.06 (405)	H-1 → L (76%)	0.0953	LFT/LMCT	
	3.13 (396)	H → L (62%) H-4 → L (14%)	0.1744	LMCT	3.39 (366)
	3.35 (371)	H-2 → L (67%)	0.0021	LFT/LMCT	
	3.45 (360)	H-4 → L (46%) H → L (27%)	0.0244	LFT/LMCT	
3F	2.61 (475)	H → L (96%)	0.0897	LFT/LMCT	2.55 (487)
	2.75 (451)	H-1 → L (96%)	0.0791	LFT/LMCT	2.85 (435)
	3.56 (349)	H → L+1 (96%)	0.0135	MLCT	
	3.60 (345)	H → L+2 (94%)	0.0177	MLCT	
3F'	3.31 (375)	H → L (80%) H-4 → L (10%)	0.0986	LMCT/LFT	
	3.55 (350)	H-1 → L (75%) H-2 → L (11%)	0.1028	LFT/LMCT	
	3.66 (338)	H-2 → L (47%) H-3 → L (31%)	0.0212	LFT/LMCT	
	3.91 (316)	H-4 → L (60%) H → L (13%)	0.0167	LFT/LMCT	

a H and L represent HOMO and LUMO, respectively. *b* Experimental data of λ_{abs} in Ref. 27.

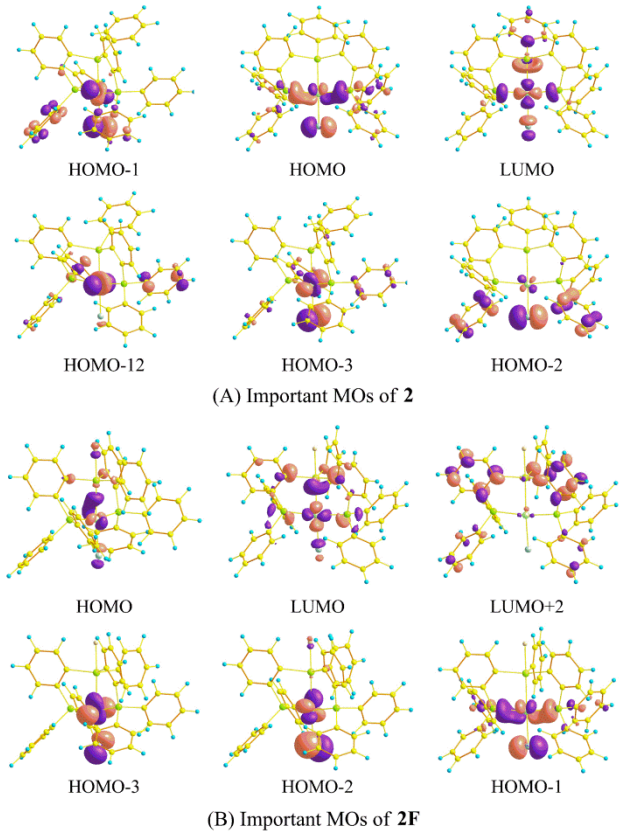

Fig. 3 Molecular orbitals of **2** and **2F** participating in the dominant electron transitions.

planar structure except for cyanide anion, as shown in Fig. S6 and S7. The reason is explained, as follows: Because the Sb-X (X = Cl, Br, or SCN) interaction is not strong enough, the Sb center does not take a completely trigonal-bipyramidal structure in [(*o*-$(Ph_2P)C_6H_4)_3SbX]^-$. As a result, the coordination of the P3 phosphine induces the strain of the (*o*-$(Ph_2P)C_6H_4)_3SbX$ (X = Cl, Br, and SCN) moiety. For instance, the (*o*-$(Ph_2P)C_6H_4)_3SbCl$ moiety in **3Cl** is more unstable than that in **3Cl'** by 8.33 kcal mol^{-1}. This strain energy is larger than the stabilization (5.76 kcal mol^{-1}) by the coordination of the third phosphine. The strain energy of the (*o*-$(Ph_2P)C_6H_4)_3SbX$ moiety is considerably large; 37.73 and 15.69 kcal mol^{-1}, for X = Br and SCN, respectively. Hence, it should be concluded that the P3 phosphine does not coordinate with the Pd center in the adducts of chloride, bromide, and thiocyanide anions. This structure should be unfavorable for spectral detection of the anion-capturing, as will be discussed below. In the case of cyanide anion (X = CN), the strain energy is 3.53 kcal mol^{-1}, which is slightly smaller than the stabilization by the P3 coordination. This is because the Sb-CN binding is somewhat strong. Actually, the allosteric coordinating system is as stable as the system without the allosteric one in the Sb-Pd combination; see **3CN** and **3CN'** in Fig. S7. In the Pt analogue, the allosteric coordinating structure is somewhat more stable than that without it; see **6CN** and **6CN'** in Fig. S7. These results suggest that the Sb-Pt combination is more favorable for the allosteric coordination than the Sb-Pd.

The above results are useful for constructing a good sensor for fluoride and cyanide anions. When one wants to detect cyanide anion, the use of the Sb-Pt combination (**6**) is recommended because the Sb-Pt combination provides a larger binding energy and induces the stronger allosteric coordination of the P3 than the Sb-Pd (**3**). When one wants to detect only fluoride anion without interference from cyanide anion, the use of the Bi-Pd combination (**5**) is recommended because the Bi-Pd can induce the allosteric coordination of the P3 only by the fluoride anion-capturing; see Table 2 and Fig. S7.

8. Absorption spectra. A good sensor for fluoride anion must possess strong anion affinity and exhibit a clear spectral change by the fluoride anion-capturing. As illustrated in Fig. 2 and listed in Table 4, the calculated absorption spectra of **2** and **3** agree with the experimental ones. The calculated absorption bands at 383 nm of **2**, 396 nm of **3**, 451 and 475 nm of **3F** are close to the experimental values; 381 nm of **2**, 366 nm of **3**, 435 and 487 nm of **3F**, respectively.[27] In **2**, all absorption peaks appear in a near ultraviolet region. Two strong absorption bands calculated at 383 and 315 nm are mainly assigned to ligand-field transitions (LFT) including a ligand-to-metal charge transfer (LMCT) character from the HOMO and the HOMO-2 to the LUMO, respectively, where it is represented as LFT/LMCT; see Fig. 3(A) for these MOs. Additional weak absorption peaks at 360 and 353 nm are also assigned to LFT/LMCT from the HOMO-1 and the HOMO-3 to the LUMO, respectively, in which the LFT character is large. In the fluoride adduct **2F**, two large absorption bands disappear but one strong band appears around 330 nm, which consists of one large (332 nm), two medium (302 and 348 nm), and one small (321 nm) absorption peaks. The strong absorption peak at 332 nm is assigned to LFT/LMCT from the HOMO-1 to the LUMO. Other weak absorption peaks at 302 and 321 are one-electron excitations of the HOMO-2 → LUMO and the HOMO-3 → LUMO, respectively. The lowest energy absorption at 348 nm is assigned to a Pd-based LFT from the HOMO to the LUMO; see Fig. 3(B). For a detailed discussion about absorption spectra of **2** and **2F**, see ESI. It should be noted that all these new absorptions are found in a near UV region. Even though some electronic photodetectors are able to observe the spectral change in this region, the visible change is much better for easy detection of the fluoride anion.

In comparison with the spectral change by the **2** → **2F** conversion, a significantly large spectral change is observed in the **3** → **3F** conversion, as shown in Fig. 2(B); **3** exhibits a large absorption at 366 nm,[27] which is calculated at 396 nm. This absorption is not observed in **2**. This band is mainly composed of one-electron excitation from the HOMO to the LUMO. Though the LUMO of **3** is essentially the same as that of **2**, the HOMO of **3** is completely different from that of **2**. The HOMO of **3** is the lone pair orbital of the free phosphine moiety, as clearly shown in Fig. 4(A). This lone pair orbital expands toward the unoccupied d_σ orbital. Hence, the LMCT transition strongly occurs. Though this assignment is different from the experimental proposal,[27] the present assignment is reasonable because the lone pair of phosphine exists at a high energy in general. Other three weak absorptions calculated at 360, 371, and 405 nm correspond to the absorptions of **2** at 353, 360, and 383 nm, respectively. The addition of fluoride anion quenches the absorption band of **3** around 400 nm but newly produces two absorption peaks in a longer wavelength region. These two peaks are transitions from

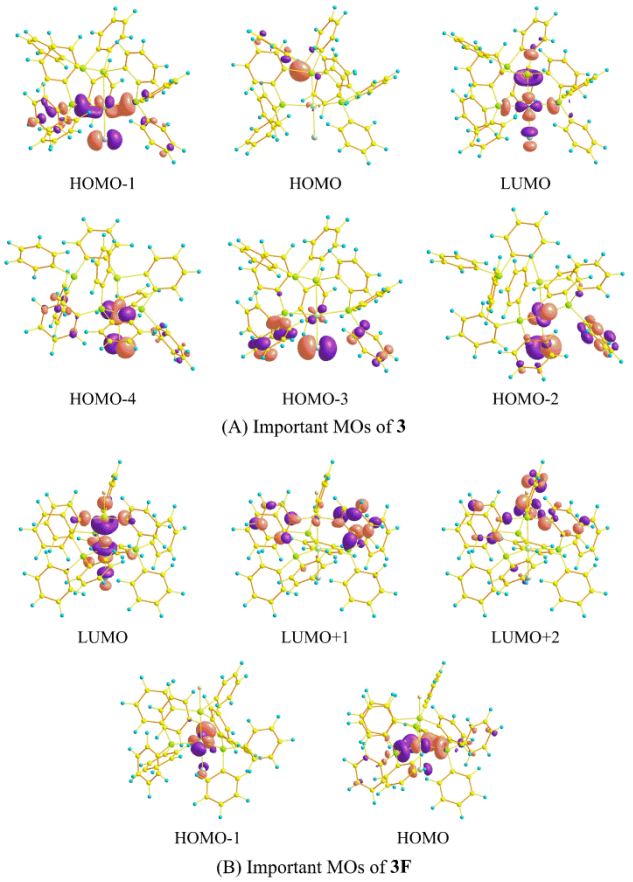

Fig. 4 Molecular orbitals of **3** and **3F** participating in the dominant electron transitions.

the HOMO and the HOMO-1 to the LUMO, which are calculated around 475 and 451 nm, respectively. The HOMO and HOMO-1 mainly consist of the Pd d_π orbital, as shown in Fig. 4(B). The LUMO is an anti-bonding MO between the Pd d_σ and the Sb lone pair orbitals. Thus, they are assigned to the Pd-center LFT consisting of $d_{xy} \rightarrow d_{z^2}$ and $d_{x^2-y^2} \rightarrow d_{z^2}$ with some of LMCT character (see Scheme 1 for the *x*, *y*, and *z*-axes). Because of the presence of a new large absorption in the visible region, it is concluded that **3** is an excellent selective colorimetric fluoride sensor, as reported experimentally.[27]

To elucidate if the allosteric coordination of the third phosphine with the Pd center is the origin of the new absorptions of **3F**, absorption spectra of three complexes **2F**, **3F**, and **3F'** are compared, as shown in Fig. 5. Complex **3F'** exhibits one absorption band around 360 nm consisting of two peaks around 375 and 350 nm. This is similar to that of **2F**. As shown in Table 4 and Fig. S8, four weak absorptions of **3F'** calculated at 375, 350, 338, and 316 nm correspond to the absorptions of **3** at 396, 405, 371, and 360 nm, respectively, due to the similar pseudo-square-planar Pd coordination structure. In the **3** → **3F** conversion, on the other hand, new absorption peaks appear in the long wavelength region, as discussed above. It is of considerable importance to elucidate the reason why **3F** exhibits a large absorption in visible region but **3F'** does not. In the trigonal-bipyramidal structure of **3F**, the d_{z^2} orbital forms anti-bonding interactions with the Sb lone pair and Cl p_σ orbitals along the *z*-axis. This is the LUMO. The d_{xy} and $d_{x^2-y^2}$ orbitals interact with

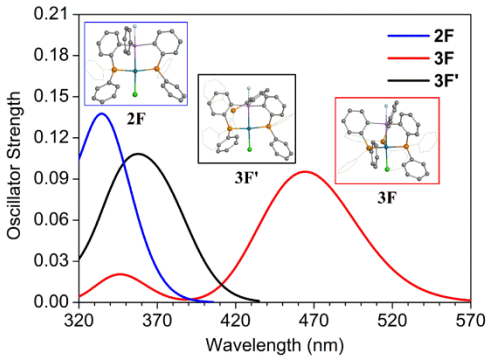

Fig. 5 Comparison of calculated absorption spectra of **2F**, **3F** and **3F'** at the PCM(CH_2Cl_2)/TD-PBE0/BS-II.

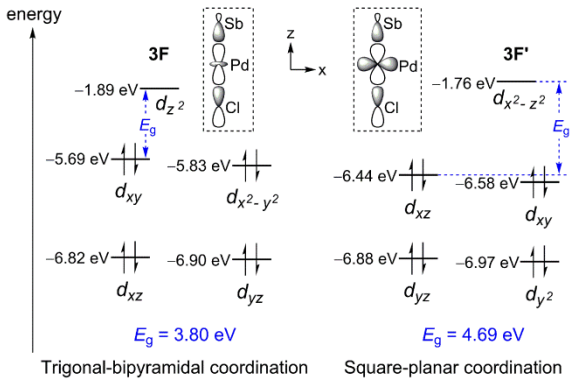

Scheme 2 Kohn-Sham orbital energies of 4d orbitals of Pd^{2+} calculated at the PCM(CH_2Cl_2)/PBE0/BS-II//PCM/PBE0/BS-I level. In dashed square boxes, modes of the anti-bonding interaction leading to destabilization of $4d_\sigma$ orbital are shown.

three phosphine lone pair orbitals in the *xy*-plane in an anti-bonding way. The non-bonding d_{xz} and d_{yz} orbitals do not undergo the anti-bonding destabilization and consequently exist at much low energy levels, as shown in Scheme 2. In the pseudo-square-planar **3F'**, on the other hand, the $d_{x^2-z^2}$ orbital exists at a much high energy due to the anti-bonding interactions with four ligands (P1, P2, Cl and Sb) along the *x*- and *z*-axes. Conversely, the other d orbitals exist at a much low energy levels because they are either non-bonding or weakly anti-bonding. As a result, the d_{xy} and $d_{x^2-y^2}$ orbitals exist at considerably higher energy in **3F** than the d_{xz} and d_{xy} orbitals in **3F'**, while the d_{z^2} orbital of **3F** exists at a lower energy than the $d_{x^2-z^2}$ orbital of **3F'**; see Scheme 2. Accordingly, d-d energy gap (E_g) is smaller in the trigonal bipyramidal **3F** than in the square-planar **3F'**. These results clearly show that the allosteric coordination of the third phosphine with the Pd center decreases the d-d energy separation, which leads to the presence of new peak in a visible region.

Because the allosteric coordination of the third phosphine with the Pd center does not occur in the cases of chloride, bromide, and thiocyanide anions (Fig. S6), the colorimetric response for these anions cannot be achieved, even if **3** can capture these anions. Based on these results, it is concluded that **3** is an excellent sensor to fluoride anion because of the large capturing ability for fluoride anion and the remarkable change of absorption spectra by fluoride binding.

9. Spectral changes in As, Bi, and Pt analogues. What changes in the spectrum occur in other complexes **5**, **6**, and **8** when

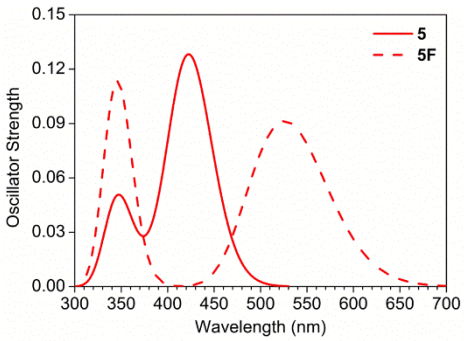

(A) Bi-Pd combination (**5** and **5F**)

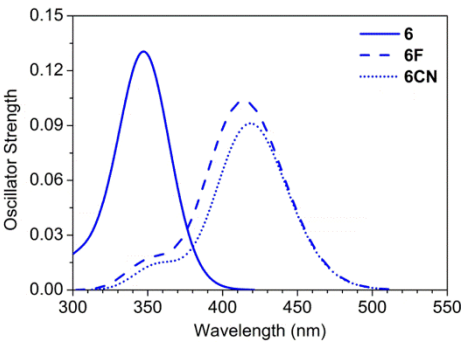

(B) Sb-Pt combination (**6**, **6F**, and **6CN**)

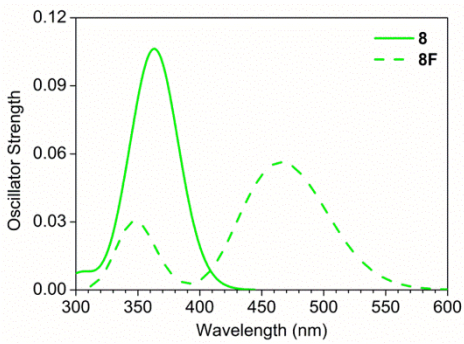

(C) Bi-Pt combination (**8** and **8F**)

Fig. 6 Calculated absorption spectra of Bi-Pd combinations **5** and **5F**, Sb-Pt combinations **6**, **6F** and **6CN**, and Bi-Pt combinations **8** and **8F** at the PCM(CH_2Cl_2)/TD-PBE0/BS-II.

capturing fluoride anion? Complexes **4** and **7** are not discussed here because of the absence of the capturing ability, as was discussed in Table 2. The calculated absorption spectra of **5**, **6**, **8**, and their fluoride adducts are plotted in Fig. 6; see Table S10 for their excitation energies and assignments and Fig. S9 for MOs participating in important transitions. Despite of the difference in fluoride capturing ability from that of **3**, these complexes exhibit similar spectral changes to those of **3F**. This is because all these complexes undergo the allosteric coordination. The Bi analogues **5** and **5F** exhibit bathochromic shift of absorption spectra, as shown in Fig. 6(A). It is noted that the fluoride anion adduct **5F** presents a large absorption peak at 546 nm, which may be easily detected. In contrast, the Pt analogues induce blue shift of absorption spectra in **6**, **6F**, **8**, and **8F**. Like **3**, the fluoride adduct formation quenches the absorption bands of **6** and **8** around 350 and 366 nm, respectively, and provides a new absorption band in the longer wavelength region, *ca*. 420 nm for **6F** and 470 nm for **8F**. These new absorption spectra are assigned to the transition-metal-center LFT/LMCT like that of **3F**. It is noted that the cyanide adduct of **6** provide a similar absorption with **6F** around 420 nm (Fig. 6(B)), indicating that **6** is also useful for sensing cyanide anion.

In conclusion, the use of Bi is effective to induce bathochromic shift. Because the Bi-Pd complex exhibits large ability for capturing fluoride anion, the Bi-Pd combination is also recommended for fluoride sensing material. Though the Pt analogue induces a blue shift, the new absorption of cyanide adduct is observed in visible region. This means that the Sb-Pt combination is useful for detecting the cyanide anion.

Conclusions

The colorimetric fluoride sensing property of the heterodinuclear main-group/transition-metal complexes $[(o\text{-}(Ph_2P)C_6H_4)_3M^1\text{-}M^2Cl]^+$ (M^1 = As, Sb, or Bi; M^2 = Pd or Pt) was systematically investigated with the DFT method. The four questions pointed out in Introduction are addressed in the following.

(1) Not only the larger F^- capturing ability of the Lewis acidic M^1 center but also the allosteric coordination of the third phosphine with the M^2 center is indispensable for the colorimetric sensing of fluoride anion. The stabilization energy by the fluoride adduct formation is −15.5 and −16.2 kcal mol^{-1} for **3** (M^1 = Sb; M^2 = Pd) and **6** (M^1 = Sb; M^2 = Pt), respectively. The formation of the hypervalent M^1-F bond induces the allosteric coordination of the P3 with the M^2 center. Accordingly, the coordination geometry of the M^2 center changes from a four-coordinate planar structure in **3**-**8** to a five-coordinate trigonal-bipyramid in fluoride adducts (**3F**-**8F**).

(2) The calculated absorption spectra agree with the experimental ones. For instance, the two absorption bands at 383 and 315 nm (**2**) disappear but a new strong peak appears at 332 nm (**2F**), when **2** converts to **2F**. These absorptions are mainly assigned to LFT/LMCT. The addition of fluoride anion to **3** quenches the absorption band around 400 nm but newly produces two absorption peaks (475 and 451 nm) in the long wavelength region in **3F**. They are assigned to the Pd-based LFT, $d_{xy} \rightarrow d_{z^2}$ and $d_{x^2-y^2} \rightarrow d_{z^2}$ including LMCT character. The allosteric coordination of the P3 with the Pd center plays a crucial role in decreasing the d-d orbital energy separation and hence the resultant spectrum appears in the visible region in the fluoride adduct.

(3) This kind of heterodinuclear complex **3** exhibits high selectivity for fluoride anion. In the anion-capturing process of **3** for such other anions as chloride, bromide and thiocyanide anions, the Pd center does not change to a trigonal-bipyramidal structure and their binding energies with those anions are only 6.0, 4.3, and 3.1 kcal mol^{-1}, respectively. The binding energy for cyanide adduct (–9.9 kcal mol^{-1}) is moderately smaller than that for the fluoride adduct, but it is enough to bind the cyanide anion. The allosteric coordination is not stable in the cyanide adduct of the Sb-Pd combination, however, in the cyanide adduct of the Sb-Pt the allosteric coordination form is more stable than the other structure without the allosteric coordination. Actually, the cyanide adduct **6CN** provides a large absorption in visible region. Thus, the Sb-Pt combination is suggested to be useful for

detecting cyanide anion.

(4) In the absence of fluoride anion, the strain energy of the bridging (o-$(Ph_2P)C_6H_4)_3Sb$ moiety of **3'** is much larger than the stabilization induced by the coordination of the third phosphine. In the fluoride adduct, on the contrary, the moderate strain energy is overcome by the Pd-P3 coordinate bond. Hence, the chelating structure of (o-$(Ph_2P)C_6H_4)_3Sb$ is the origin of the absence of the P3 allosteric coordination in **3** but the presence of the P3 coordination in **3F**; in other words, this ligand plays a crucial role in the allosteric coordination.

The Bi-Pd (**5**) and Bi-Pt (**8**) combinations provide a moderately smaller binding energies (–10.5 and –10.9 kcal mol^{-1}) than that of **3**, and the Sb-Pt combination (**6**) presents a bit larger binding energy (–16.2 kcal mol^{-1}) than **3**. Also, **5**, **6**, and **8** exhibit similar spectral changes to those of the **3** → **3F** conversion because of the allosteric coordination on the Pd/Pt center in the fluoride adduct. The Bi-Pd combination is recommended for fluoride sensing material without interference from cyanide anion.

In addition to the theoretical answers for four questions, we wish to mention here characteristic features of the hypervalent Sb species. Our calculations clearly show that the stibine (SbR_3) is less electron-donating than the silyl (SiR_3) but the hypervalent Sb species (SbR_3F^-) is stronger electron-donating and exhibits stronger *trans*-influence than the silyl. Because the silyl is a typical strongly donating ligand with strong *trans*-influence, this feature of the hypervalent Sb species is of considerable interest in the coordination chemistry; for instance, the ligand field in the transition-metal stibine complex is enhanced very much by addition of fluoride anion.

Acknowledgments

This work is financially supported by the Grant-in-Aids from Ministry of Education, Culture, Science, Sport, and Technology through Grant-in-Aids of Specially Promoted Science and Technology (no. 22000009) and Grand Challenge Project (IMS).

Notes and references

Fukui Institute for Fundamental Chemistry, Kyoto University, Takano-Nishihiraki-cho 34-4, Sakyo-ku, Kyoto 606-8103, Japan. E-mail: sakaki.shigeyoshi.47e@st.kyoto-u.ac.jp

† Electronic Supplementary Information (ESI) available: Fig. S1 (model systems **2$_m$**, **2$_m$F**, **3$_m$**, **3$_m$F** and **2$_m$Si**), Fig. S2-S4 (complex **4**, **4F**, **4F'**, **5**, **5F**, **5F'**, **6**, **6F**, **6F'**, **7**, **7F**, **7F'**, **8**, **8F**, and **8F'** geometries), Fig. S5 (optimized structures of $SbPh_3$ and $[NMe_4]FSbPh_3$), Fig. S6-S7 (structures and relative energies of **3Cl**, **3Cl'**, **3Br**, **3Br'**, **3SCN**, **3SCN'**, **3CN**, **3CN'**, **5CN, 5CN'**, **6CN**, and **6CN'**), Fig. S8 and S9 (MOs for **3F'**, **5**, **6**, **8** and their fluoride adducts), Fig. S10 (MEPs of **1, 2** and **3**), Fig. S11 (four isomers of **3**[BMe_4]), Scheme S1 (structure and representations of five d orbitals for **2**), Tables S1-S4 (functional test), Tables S5-S7 (structural parameters of **1**, **1F**, **2**, **2F**, **3**, and **3F**), Table S8 (WBI of **1**-**3** and their F^- adducts), Table S9 (natural population of **2$_{mSi}$**, **2$_m$**, **2$_m$F**, **3$_m$**, and **3$_m$F**), Table S10 (absorption peaks, the oscillator strength, and assignments for **5**, **5F**, **6**, **6F**, **6CN**, **8**, and **8F**), and Cartesian coordinates of the optimized geometries. See DOI: 10.1039/b000000x/

1 K. L. Kirk, *Biochemistry of the Elemental Halogens and Inorganic Halides*, Plenum Press: New York, 1991.
2 W. Czarnowski, J. Kerchniak, B. Urbanska, K. Stolarska, M. Taraszewska and A. Muraszko, *Fluoride*, 1999, **32,** 91.
3 E. B. Bassin, D. Wypij and R. B. Davis, *Cancer Causes Control*, 2006, **17**, 421.
4 T. Gunnlaugsson, M. Glynn, G. M. Tocci, P. E. Kruger and F. M. Pfeffer, *Coord. Chem. Rev.*, 2006, **250**, 3094.
5 T. W. Hudnall, C.-W. Chiu and F. P. Gabbaï, *Acc. Chem. Res.*, 2009, **42**, 388.
6 M. Cametti and K. Rissanen, *Chem. Commun.*, 2009, 2809.
7 Q. Zhao, F. Y. Li and C. H. Huang, *Chem. Soc. Rev.*, 2010, **39**, 3007.
8 J. S.Wu, W. M. Liu, J. C. Ge, H. Y. Zhang and P. F. Wang, *Chem. Soc. Rev.*, 2011, **40**, 3483.
9 H. Miyaji, W. Sato and J. L. Sessler, *Angew. Chem. Int. Ed.*, 2000, *39*, 1777.
10 M. D. Best, S. L. Tobey and E. V. Anslyn, *Coord. Chem. Rev.*, 2003, **240**, 3.
11 J. L. Sessler, S. Camiolo and P. A. Gale, *Coord. Chem. Rev.*, 2003, **240**, 17.
12 J. M. Llinares, D. Powell and K. Bowman-James, *Coord. Chem. Rev.*, 2003, **240**, 57.
13 C. R. Bondy and S. J. Loeb, *Coord. Chem. Rev.*, 2003, **240**, 77.
14 K. Choi and A. D. Hamilton, *Coord. Chem. Rev.*, 2003, **240**, 101.
15 M. Boiocchi, L. Del Boca, D. E. Gómez, L. Fabbrizzi, M. Licchelli and E. Monzani, *J. Am. Chem. Soc.*, 2004, **126**, 16507.
16 D. A. Jose, D. K. Kumar, B. Ganguly and A. Das, *Org. Lett.*, 2004, **6**, 3445.
17 S. P. Mahanta, B. S. Kumar, S. Baskaran, C. Sivasankar and P. K. Panda, *Org. Lett.*, 2012, **14**, 548.
18 S. Yamaguchi, S. Akiyama and K. Tamao, *J. Am. Chem. Soc.*, 2000, **122**, 6793.
19 Y. Kim, M. Kim and F. P. Gabbaï, *Org. Lett.*, 2010, **12**, 600.
20 C. R. Wade, T.-P. Lin, R. C. Nelson, E. A. Mader, J. T. Miller and F. P. Gabbaï, *J. Am. Chem. Soc.*, 2011, **133**, 8948.
21 S. Yamaguchi, S. Akiyama and K. Tamao, *J. Am. Chem. Soc.*, 2001, **123**, 11372.
22 Z. M. Hudson and S. N. Wang, *Acc. Chem. Res.*, 2009, **42**, 1584.
23 C. R. Wade, A. E. J. Broomsgrove, S. Aldridge and F. P. Gabbaï, *Chem. Rev.*, 2010, **110**, 3958.
24 F. Jäkle, *Chem. Rev.*, 2010, **110**, 3985.
25 H. Y. Zhao and F. P. Gabbaï, *Organometallics*, 2012, **31**, 2327.
26 V. Amendola and L. Fabbrizzi, *Chem. Commun.*, 2009, 513.
27 C. R. Wade, I.-S. Ke and F. P. Gabbaï, *Angew. Chem. Int. Ed.*, 2012, **51**, 478.
28 (*a*) K. Toyota, Y. Yamamoto and K. Akiba, *J. Chem. Res. (s)*, 1999, 386; (*b*) K. Toyota, Y. Yamamoto and K. Akiba, *Chem. Lett.*, 1999, 783; (*c*) K. Toyota, Y. Yamamoto and K. Akiba, *J. Organomet. Chem.*, 1999, **586**, 171; (*d*) Y. Yamamoto, K. Toyota, Y. Wakisaka and K. Akiba, *Heteroatom Chem.*, 2000, **11**, 42; (*e*) K. Toyota, Y. Wakisaka, Y. Yamamoto and K. Akiba, *Organometallics*, 2000, **19**, 5122; (*f*) K. Toyota, Y. Yamamoto and K. Akiba, *Organometallics*, 2000, **19**, 5134.
29 (*a*) J. Wagler, A. F. Hill, T. Heine, *Eur. J. Inorg. Chem.*, 2008, 4225; (*b*) J. Wagler and E. Brendler, *Angew. Chem. Int. Ed.*, 2010, **49**, 624; (*c*) L. A. Truflandier, E. Brendler, J. Wagler and J. Autschbach, *Angew. Chem. Int. Ed.*, 2011, **50**, 255; (*d*) E. Brendler, E. Wächtler, T. Heine, L. Zhechkov, T. Langer, R. Pöttgen, A. F. Hill and J. Wagler, *Angew. Chem. Int. Ed.*, 2011, **50**, 4696.
30 (*a*) P. Gualco, T.-P. Lin, M. Sircoglou, M. Mercy, S. Ladeira, G. Bouhadir, L. M. Pérez, A. Amgoune, L. Maron, F. P. Gabbaï, D. Bourissou, *Angew. Chem. Int. Ed.*, 2009, **48**, 9892; (*b*) T.-P. Lin, C. R. Wade, L. M. Pérez, F. P. Gabbaï, *Angew. Chem. Int. Ed.*, 2010, **49**, 6357.
31 P. Gualco, M. Mercy, S. Ladeira, Y. Coppel, L. Maron, A. Amgoune, D. Bourissou, *Chem. Eur. J.*, 2010, **16**, 10808.
32 K. Junold, J. A. Baus, C. Burschka and R. Tacke, *Angew. Chem. Int. Ed.*, 2012, **51**, 7020.
33 S. Sakaki, D. Kawai and S. Tsukamoto, *Collect. Czech. Chem. Commun.*, 2011, **76**, 619.
34 T.-P. Lin and F. P. Gabbaï, *J. Am. Chem. Soc.*, 2012, **134**, 12230.
35 Using tight criteria for geometry optimization and wave function convergence combined with ultrafine grid.
36 M. J. Frisch, G. W. Trucks, H. B. Schlegel, G. E. Scuseria, M. A. Robb, J. R. Cheeseman, G. Scalmani, V. Barone, B. Mennucci, G. A. Petersson, H. Nakatsuji, M. Caricato, X. Li, H. P. Hratchian, A. F. Izmaylov, J. Bloino, G. Zheng, J. L. Sonnenberg, M. Hada, M. Ehara, K. Toyota, R. Fukuda, J. Hasegawa, M. Ishida, T. Nakajima, Y. Honda, O. Kitao, H. Nakai, T. Vreven, J. A. Montgomery, Jr., J. E.

Peralta, F. Ogliaro, M. Bearpark, J. J. Heyd, E. Brothers, K. N. Kudin, V. N. Staroverov, R. Kobayashi, J. Normand, K. Raghavachari, A. Rendell, J. C. Burant, S. S. Iyengar, J. Tomasi, M. Cossi, N. Rega, J. M. Millam, M. Klene, J. E. Knox, J. B. Cross, V. Bakken, C. Adamo, J. Jaramillo, R. Gomperts, R. E. Stratmann, O. Yazyev, A. J. Austin, R. Cammi, C. Pomelli, J. W. Ochterski, R. L. Martin, K. Morokuma, V. G. Zakrzewski, G. A. Voth, P. Salvador, J. J. Dannenberg, S. Dapprich, A. D. Daniels, Ö. Farkas, J. B. Foresman, J. V. Ortiz, J. Cioslowski and D. J. Fox, Gaussian 09, Revision B.01, Gaussian, Inc., Wallingford CT, 2009.

37 J. P. Perdew, K. Burke and M. Ernzerhof, *Phys. Rev. Lett.*, 1996, **77**, 3865.

38 J. P. Perdew, K. Burke and M. Ernzerhof, *Phys. Rev. Lett.*, 1997, **78**, 1396.

39 C. Adamo and V. Barone, *J. Chem. Phys.*, 1999, **110**, 6158.

40 M. Couty and M. B. Hall, *J. Comp. Chem.*, 1996, **17**, 1359.

41 A. W. Ehlers, M. Böhme, S. Dapprich, A. Gobbi, A. Höllwarth, V. Jonas, K. F. Köhler, R. Stegmann, A. Veldkamp and G. Frenking, *Chem. Phys. Lett.*, 1993, **208**, 111.

42 A. Höllwarth, M. Böhme, S. Dapprich, A. W. Ehlers, A. Gobbi, V. Jonas, K. F. Köhler, R. Stegmann, A. Veldkamp and G. Frenking, *Chem. Phys. Lett.*, 1993, **208**, 237.

43 P. J. Hay and W. R. Wadt, *J. Chem. Phys.*, 1985, **82**, 270.

44 W. R. Wadt and P. Hay, *J. Chem. Phys.*, 1985, **82**, 284.

45 P. J. Hay and W. R. Wadt, *J. Chem. Phys.*, 1985, **82**, 299.

46 K. A. Peterson, *J. Chem. Phys.*, 2003, **119**, 11099.

47 B. Metz, H. Stoll and M. Dolg, *J. Chem. Phys.*, 2000, **113**, 2563.

48 T. H. Dunning, Jr., *J. Chem. Phys.*, 1989, **90**, 1007.

49 D. E. Woon and T. H. Dunning, Jr., *J. Chem. Phys.*, 1993, **98**, 1358.

50 A. K. Wilson, D. E. Woon, K. A. Peterson and T. H. Dunning, Jr., *J. Chem. Phys.*, 1999, **110**, 7667.

51 J. Tomasi, B. Mennucci and R. Cammi, *Chem. Rev.*, 2005, **105**, 2999.

52 N. M. O'boyle, A. L. Tenderholt and K. M. Langner, *J. Comp. Chem.*, 2008, **29**, 839.

53 In the model system $[PdCl(SbPh_3F)(PH_3)_2]$, the Pd-P distance is slightly shortened despite that the σ-donation of phosphine becomes weak. The reason is not clear at this moment.

54 The difference in the strain energy of the $(o\text{-}(Ph_2P)C_6H_4)_3Sb$ moiety between **3** and **3'** was calculated as the energy difference between the corresponding free $(o\text{-}(Ph_2P)C_6H_4)_3Sb$ groups with the same geometries as those of **3** and **3'**. Then, applying the equation, $\Delta E_{relative}[\mathbf{3'}–\mathbf{3}] = E_{strain}[(o\text{-}(Ph_2P)C_6H_4)_3Sb] + E_{stabilization}$[Pd-P3 coordination], we evaluated the stabilization energy by the coordination of the third phosphine. A similar methodology was applied for the other compounds discussed in the text.